

# Variable Band Gap Poly(arylene ethynylene) Conjugated Polyelectrolytes

Xiaoyong Zhao, Mauricio R. Pinto, Lindsay M. Hardison, Jeremiah Mwaura, Juergen Müller, Hui Jiang, David Witker, Valeria D. Kleiman, John R. Reynolds,\* and Kirk S. Schanze\*

Department of Chemistry, University of Florida, P.O. Box 117200, Gainesville, Florida 32611-7200

Received May 22, 2006; Revised Manuscript Received July 10, 2006

**ABSTRACT:** A series of poly(arylene ethynylene) (PAE) conjugated polyelectrolytes (CPEs) have been prepared using palladium-mediated (Sonogashira) coupling chemistry. The series consists of five pairs of polymers that share the same poly(arylene ethynylene) backbone. One member of each pair contains anionic sulfonate ( $\text{R}-\text{SO}_3^-$ ) side groups, whereas the other member contains cationic bis-alkylammonium ( $\text{R}-\text{N}^+-\text{R}-\text{N}^+-\text{R}$ ) side groups. The repeat unit structure of the poly(arylene ethynylene) backbone consists of a bis(alkoxy)phenylene-1,4-ethynylene unit alternating with a second arylene ethynylene moiety, and five different aryls were used, Ar = 1,4-phenyl, 2,5-pyridyl (Py), 2,5-thienyl (Th), 2,5-(3,4-ethylenedioxy)thienyl (EDOT), and 1,4-benzo[2,1,3]-thiodiazole (BDT). The different arylene units induce variation in the HOMO–LUMO band gap across the series of polymers, resulting in a series of materials that display absorption maxima at wavelengths ranging from 400 to 550 nm and fluorescence maxima ranging from 440 to 600 nm. The absorption and fluorescence properties of the CPEs were investigated in methanol, water, and in methanol/water mixtures. The photophysical data suggest that the CPE chains aggregate in water, but in methanol, the polymers are well solvated such that the optical properties are characteristic of the “molecularly dissolved” chains. Stern–Volmer (SV) fluorescence quenching studies were carried out using ionic naphthalene diimides as electron acceptors. The results show that the fluorescence from the CPEs was quenched with very high efficiency (amplified quenching) when the ionic diimide was charged opposite to the charge on the CPE chain. The sensitivity of the Stern–Volmer quenching response varies strongly across the series of CPEs, with the most efficient quenching seen for polymers that display efficient fluorescence when they are aggregated. The relationship between CPE side chain structure, band gap, fluorescence quantum yield, extent of chain aggregation, and fluorescence quenching efficiency is discussed.

## Introduction

Conjugated polyelectrolytes (CPEs) have been the focus of significant interest during the past decade.<sup>1,2</sup> Research on this class of conjugated polymers has been stimulated by their remarkable materials properties. In particular, because of the presence of ionic solubilizing groups, CPEs are water soluble yet they retain the optical and electronic properties characteristic of the  $\pi$ -conjugated polymer backbone.<sup>3–9</sup> In addition, because of the combination of ionic charged groups and significant hydrocarbon content, CPEs are amphiphilic, and therefore, they have a strong propensity to self-assemble into aggregates in solution.<sup>5,10–12</sup>

Many CPEs are strongly fluorescent in the visible region. This fluorescence is quenched very efficiently by low concentrations of electron- or energy-transfer quenchers that feature an ionic charge that is opposite to that of the CPE.<sup>4,5,13–15</sup> This effect, which is referred to as “amplified quenching”,<sup>16</sup> arises due to a combination of two effects. First, the oppositely charged quencher ions associate with the CPE chains by ion-pairing.<sup>14</sup> Second, the fluorescent exciton is delocalized on the  $\pi$ -conjugated polymer, and it is able to undergo very rapid intra- and interchain diffusion.<sup>15,17</sup> Several studies have probed the mechanism of amplified quenching in different CPE quencher systems.<sup>14,15,17</sup> These studies have uncovered the various factors that lead to high quenching efficiency, including the stability of the polymer–quencher ion-pair complex and the ability of polyvalent quencher ions to induce aggregation of the polymer chains.

We are engaged in an ongoing investigation that seeks to explore the fundamental properties and applications of CPEs, including understanding the mechanism of inter- and intrachain energy transport and amplified quenching,<sup>15,17</sup> as well as the use of the materials in nanostructured photovoltaic cells fabricated by the layer-by-layer (LbL) approach.<sup>18</sup> As part of this investigation, we sought to develop a general synthetic approach to a family of structurally related CPEs of varying optical band gap that feature cationic and anionic solubilizing groups. To accomplish this objective, we utilized the Sonogashira coupling method<sup>19,20</sup> to prepare cationic and anionic CPEs with poly(arylene ethynylene) (PAE) backbones containing a variety of different aryl units in the  $\pi$ -conjugated backbone. The different aryl units give rise to materials with a wide range of HOMO–LUMO gaps. In the present manuscript, we provide a detailed report of this work, including a summary of the synthetic methods used to prepare and purify the polymers, along with results of a photophysical study that examines the absorption and fluorescence spectroscopy and fluorescence quenching of the polymers in several different solvents. This study is the first to examine the properties of a homologous family of CPEs that differ widely in HOMO–LUMO band gap. The results show that it is possible to tune the energy of the fluorescent exciton by varying the nature of the aryl units in the polyelectrolyte’s poly(arylene ethynylene) backbone while preserving the intrinsic solution properties of the polymers.

## Experimental Section

**Instrumentation and Methods.** NMR spectra were recorded using a Varian VXR-300 FT-NMR, operating at 300 MHz for  $^1\text{H}$  NMR and at 75.4 MHz for  $^{13}\text{C}$  NMR. FTIR spectra were obtained with a Perkin-Elmer 1600 spectrometer. UV–Visible absorption

\*Corresponding authors. E-mail: kschanze@chem.ufl.edu (K.S.S.). Telephone: 352-392-9133. Fax: 352-392-2395.

spectra were recorded using a Varian Cary 100 dual beam spectrophotometer with a scan rate of 300 nm/min. Corrected steady-state fluorescence spectra were obtained with a SPEX Fluorolog-3 spectrometer. A 1 cm square quartz cuvette was used for solution spectra, and emission was collected at 90° relative to excitation beam. Fluorescence quantum yields are reported relative to known standards. The optical density of solutions at the excitation wavelength was  $\leq 0.1$ , and corrections were applied for differences in the refractive index of standard and sample solutions.

**General Synthesis.** Tetrahydrofuran and triethylamine were distilled over sodium hydride under nitrogen prior to use. Dichloromethane was distilled over phosphorus pentoxide. 3,4-Ethylenedioxythiophene (Bayer) was distilled under reduced pressure. 2,5-Dibromothiophene, 2,5-dibromopyridine, 2,1,3-benzothiadiazole (BDT), 1 M tetrabutylammonium fluoride THF solution (Aldrich), copper(I) iodide, iodine monochloride, diisopropylamine (Acros), trimethylsilylacetylene (GFS), and tetrakis(triphenylphosphine)-palladium(0) (Strem) were used as received. All other analytical-grade chemicals and solvents were used without any further treatment. Iodine monochloride–pyridine complex,<sup>21</sup> 1,4-diethynylbenzene,<sup>22</sup> 4,7-diethynyl-2,1,3-benzothiadiazole,<sup>23</sup> 2,5-diethynylpyridine,<sup>24</sup> 2,5-diethynylthiophene,<sup>25</sup> 1,4-diiodo-2,5-bis(2-bromoethoxy)benzene,<sup>12</sup> and 3,3'-[(2,5-diiodo-1,4-phenylene)bis(oxy)]bis-(1-propanesulfonic acid) disodium salt (**1**),<sup>5</sup> were synthesized and purified according to procedures published elsewhere. PPE–SO<sub>3</sub><sup>−</sup> was prepared and characterized as reported previously.<sup>5</sup>

**2,5-Diiodo-3,4-ethylenedioxythiophene (2).** A solution of 5.6 g (40.0 mmol) of 3,4-ethylenedioxythiophene and 23.0 g (90.0 mmol) of iodine monochloride–pyridine complex in 150 mL of dry dichloromethane was stirred at room temperature for 1 h. A precipitate of pyridinium salt that was produced during the reaction was removed by vacuum filtration, and the filtrate was evaporated. The remaining solid residue was rinsed with a mixture of water/methanol 1:1, and it was recrystallized twice from acetone. The product was obtained as greenish-white crystals, yield 14.8 g (93%). <sup>1</sup>H NMR (DMSO-*d*<sub>6</sub>;  $\delta$  ppm from TMS): 4.25 (s, 4H). <sup>13</sup>C NMR (DMSO-*d*<sub>6</sub>;  $\delta$  ppm from TMS): 54.08, 64.83, 143.84. Elemental analysis calcd for C<sub>6</sub>H<sub>4</sub>I<sub>2</sub>O<sub>2</sub>S: C, 18.29; H, 1.02. Found: C, 18.41; H, 0.77.

**2,5-Bis(trimethylsilylethynyl)-3,4-ethylenedioxythiophene (3).** A deoxygenated solution of 3.93 g (10.0 mmol) of **2**, 6 mL (42.6 mmol) of trimethylsilylacetylene, 580 mg (0.5 mmol) of Pd(PPh<sub>3</sub>)<sub>4</sub>, and 95 mg (0.5 mmol) of CuI in 20 mL of THF/Et<sub>3</sub>N 2:1 mixture was stirred at room temperature under argon for 2 h. The triethylammonium salt that precipitated during the reaction was removed by filtration, and the filtrate was evaporated by vacuum distillation. The remaining dark oil was eluted through a silica gel column with hexane. The pale-yellow hexane solution was evaporated, and the solid obtained was recrystallized two times from 90% methanol. The product was obtained as a fine light-yellow solid, yield 1.27 g (38%). <sup>1</sup>H NMR (CDCl<sub>3</sub>;  $\delta$  ppm from TMS): 0.24 (s, 18H), 4.26 (s, 4H). <sup>13</sup>C NMR (CDCl<sub>3</sub>;  $\delta$  ppm from TMS): 0.12, 64.97, 94.39, 99.91, 103.12, 143.79. Elemental analysis calcd for C<sub>16</sub>H<sub>22</sub>O<sub>2</sub>SSi<sub>2</sub>: C, 57.44; H, 6.63. Found: C, 57.22; H, 6.32.

**2,5-Diethynyl-3,4-ethylenedioxythiophene (4).** A solution of 1.0 g (3.0 mmol) of **3** in 20 mL of dioxane was acidified with 2 mL of 50% acetic acid and then deoxygenated with purging argon for 10 min. Then 25 mL of a solution of *n*-Bu<sub>4</sub>NF THF (*c* = 1 M) was added, and the resulting mixture was stirred for 30 min at room temperature. Half of the solution volume was evaporated, and the resulting solution was poured into 300 mL of ice water. The precipitated solid was collected by vacuum filtration, dissolved in 50 mL of hexanes, and eluted through a short plug of silica gel. The solvent was evaporated, and the solid obtained was stored in a refrigerator for a few hours prior to use. Note that this compound rapidly decolorizes if stored even for relatively short periods of time. <sup>1</sup>H NMR (CDCl<sub>3</sub>;  $\delta$  ppm from TMS): 3.50 (s, 2H), 4.30 (s, 4H). <sup>13</sup>C NMR (CDCl<sub>3</sub>;  $\delta$  ppm from TMS): 65.04, 73.96, 85.06, 98.70, 144.37. Elemental analysis calcd for C<sub>10</sub>H<sub>6</sub>O<sub>2</sub>S: C, 63.14; H, 3.18. Found: C, 62.82; H, 3.05.

**1-Hexyl-4-aza-1-azoniabicyclo[2.2.2]octane Bromide (5).** Diazabicyclo[2.2.2]octane (10.0 g, 89.2 mmol) and hexyl bromide (6.3 mL, 44.6 mmol) were combined in 100 mL of ethyl acetate. The solution was stirred for 24 h, after which time, a white precipitate had formed. The solid was collected by vacuum filtration, rinsed with ethyl acetate, and dried under vacuum, yield 11.23 g (91%). <sup>1</sup>H NMR (DMSO-*d*<sub>6</sub>;  $\delta$  ppm): 0.87 (t, 3 H), 1.28 (m, 6 H), 1.64 (m, 2 H), 3.01 (t, 6 H), 3.22 (m, 2 H), 3.32 (t, 6 H).

**4,4'-(2,2'-(2,5-Diiodo-1,4-phenylene)bis(oxy))bis(ethane-2,1-diyl)bis(1-hexyl-1,4-diazonia-bicyclo[2.2.2]octane) Tetrabromide (6).** A solution of 5.8 g (10 mmol) of 1,4-diiodo-2,5-bis(2-bromoethoxy)benzene and 7.0 g (25 mmol) of **5** in 100 mL of dimethylacetamide was stirred at 110 °C for 6 h. Upon cooling, 200 mL of cold ether was added to the reaction mixture. The resulting white precipitate was collected by filtration and recrystallized twice from water, yield 9.8 g (86%). <sup>1</sup>H NMR (DMSO-*d*<sub>6</sub>;  $\delta$  ppm): 0.87 (t, 6 H), 1.32 (m, 12 H), 1.72 (m, 4 H), 3.59 (m, 4 H), 3.98 (t, 12 H), 4.14 (m, 16 H), 4.55 (m, 4 H), 7.57 (s, 1 H). <sup>13</sup>C NMR (DMSO-*d*<sub>6</sub>;  $\delta$  ppm): 13.83, 21.25, 21.80, 25.17, 30.59, 50.27, 51.38, 62.59, 63.12, 63.33, 87.16, 123.09, 152.11. Elemental analysis calcd for C<sub>34</sub>H<sub>60</sub>Br<sub>4</sub>I<sub>2</sub>N<sub>4</sub>O<sub>2</sub>: C, 36.13; H, 5.35; N, 4.96. Found: C, 35.19; H, 5.60; N, 4.61.

**Polymerization Reactions.** All of the polymers were prepared from the corresponding monomers to a similar procedure. Representative procedures for anionic and cationic polymers are provided below.

**PPE-EDOT–SO<sub>3</sub><sup>−</sup>.** A deoxygenated solution of 69 mg (60  $\mu$ mol) of Pd(PPh<sub>3</sub>)<sub>4</sub> and 11 mg (60  $\mu$ mol) of CuI in 25 mL of DMF/diisopropylamine 1:1 mixture was added via cannula to a deoxygenated solution of 0.380 g (2.00 mmol) of **4** and 1.300 g (2.00 mmol) of 3,3'-[(2,5-diiodo-1,4-phenylene)bis(oxy)]bis-(1-propanesulfonic acid) disodium salt (**1**) in 150 mL of a DMF/water mixture (1:1 v/v) contained in a Schlenk flask. The resulting solution was purged with argon for 10 min and then stirred at 60 °C for 12 h. The polymerization reaction was terminated by pouring the reaction mixture into 600 mL of methanol/acetone/diethyl ether (1:3:3 v/v/v). The precipitated polymer was collected by vacuum filtration and redissolved in 50 mL of water. To this solution 0.1 g of NaCN was added, and then the solution was filtered through a 0.8  $\mu$ m nylon membrane. The polymer was again precipitated from the filtered solution by pouring into a methanol/acetone/diethyl ether mixture (1:3:3 v/v/v). Final purification was accomplished by dialysis of an aqueous solution of the polymer against deionized water (Millipore Simplicity water system) using a 6–8 kD MWCO cellulose membrane (Fisher Scientific). After dialysis, the polymer solution was filtered through a 0.45  $\mu$ m nylon membrane, and the concentration was adjusted to ca. 1.0 mg mL<sup>−1</sup>. The polymer was stored in this format and diluted as appropriate for spectroscopic studies. Yield: 950 mg (81%). <sup>1</sup>H NMR (DMSO-*d*<sub>6</sub>;  $\delta$  ppm): 2.08 (br, 4H), 2.71 (br, 4H), 4.14 (br, 4H), 4.44 (br, 4H), 7.08 (s, 2H). FTIR ( $\nu_{\text{max}}$ , cast film): 2941, 2878, 2196, 1621 (broad), 1489, 1472, 1446, 1417, 1366, 1276, 1192 (broad), 1082, 1047, 961, 850, 794, 739, 612, 527.

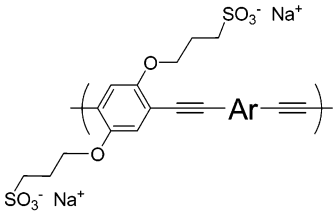
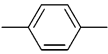
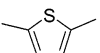
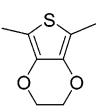
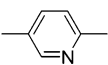
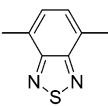
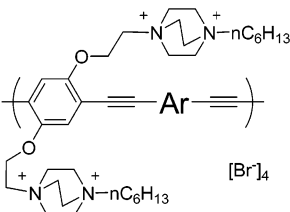

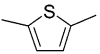
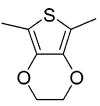
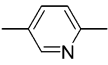
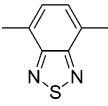
**PPE-Th–SO<sub>3</sub><sup>−</sup>.** <sup>1</sup>H NMR (DMSO-*d*<sub>6</sub>;  $\delta$  ppm): 2.15 (br, 4H), 2.68 (br, 4H), 4.14 (br, 4H), 7.13 (br, 2H), 7.35 (br, 2H). FTIR ( $\nu_{\text{max}}$ , cast film): 3096, 2947, 2878, 2194, 1644 (broad), 1531, 1492, 1470, 1447, 1411 (sh), 1382, 1279, 1195 (broad), 1047, 937, 916 (sh), 855, 802, 737, 716 (sh), 614, 534.

**PPE-Py–SO<sub>3</sub><sup>−</sup>.** <sup>1</sup>H NMR (DMSO-*d*<sub>6</sub>;  $\delta$  ppm): 2.11 (br, 4H), 2.70 (br, 4H), 4.21 (br, 4H), 7.26 (s, 2H), 7.71 (br, 1H), 7.99 (br, 1H), 8.77 (s, 1H). FTIR ( $\nu_{\text{max}}$ , cast film): 2946, 2882, 2208, 1719 (sh), 1644, 1586, 1543, 1505, 1475, 1443, 1420, 1383, 1365 (sh), 1282, 1199 (broad), 1045, 946, 842, 796, 751 (sh), 737, 614, 529.

**PPE-BTD–SO<sub>3</sub><sup>−</sup>.** <sup>1</sup>H NMR (DMSO-*d*<sub>6</sub>;  $\delta$  ppm): 2.6–3.0 (aliphatic C–H), 3.6–4.0 (aliphatic C–H), 7.2–8.2 (aromatic C–H). FTIR ( $\nu_{\text{max}}$ , cast film): 2946, 2877, 2205, 1644 (broad), 1559, 1537, 1512, 1487, 1440, 1419, 1385, 1343, 1282, 1186 (broad), 1046, 891, 847, 799, 736, 632, 614, 566, 526.

**PPE-EDOT–(4+).** A deoxygenated solution of 69 mg (60  $\mu$ mol) of Pd(PPh<sub>3</sub>)<sub>4</sub> and 11 mg (60  $\mu$ mol) of CuI in 25 mL of DMF/diisopropylamine 1:1 mixture was added via cannula to a deoxy-

Table 1. Structures and Intrinsic Viscosity for PPE-Type Conjugated Polyelectrolytes

Polymer Structure	Ar	Acronym	$[\eta]$ dL·g <sup>-1</sup> <sup>a</sup>
		PPE-SO <sub>3</sub> <sup>-</sup>	3.84
		PPE-Th-SO <sub>3</sub> <sup>-</sup>	1.03
		PPE-EDOT-SO <sub>3</sub> <sup>-</sup>	0.81
		PPE-Py-SO <sub>3</sub> <sup>-</sup>	0.72
		PPE-BDT-SO <sub>3</sub> <sup>-</sup>	0.96
		PPE-(4+)	1.63
		PPE-Th-(4+)	0.47
		PPE-EDOT-(4+)	0.29
		PPE-Py-(4+)	0.50
		PPE-BDT-(4+)	0.33

<sup>a</sup> Intrinsic viscosity measured in 0.1 M LiBr/DMSO solution at 20 °C.

generated solution of 0.380 g (2.00 mmol) of **4** and 1.62 g (2.00 mmol) of **6** in 150 mL of a DMF/water mixture (1:1 v/v) contained in a Schlenk flask. The resulting solution was purged with argon for 10 min and then stirred at 70 °C for 24 h. After cooling, the polymerization reaction was terminated by pouring the reaction mixture into 700 mL of diethyl ether/acetone/methanol (3:1:1 v/v/v). The precipitated polymer was collected by vacuum filtration and redissolved in 50 mL of DMF/water (2:1 v/v). (This solution was not treated with NaCN.) The polymer was again precipitated by addition to 700 mL of diethyl ether/acetone/methanol. The precipitate was isolated by filtration, and it was purified by dialysis as described above for PPE-EDOT-SO<sub>3</sub><sup>-</sup>. After dialysis, the polymer solution was filtered through a 0.45 μm nylon membrane, and the concentration was adjusted to ca. 1.0 mg mL<sup>-1</sup>. The polymer was stored in this format and diluted as appropriate for spectroscopic studies. <sup>1</sup>H NMR (DMSO-*d*<sub>6</sub>; δ ppm): 0.89 (br, 6H), 1.34 (br, 12H), 1.77 (br, 4H), 3.73 (br, 4H), 4.21–4.33 (br, 28H), 4.58 (br, 4H), 4.70 (br, 4H), 7.37 (br, 2H). FTIR ( $\nu_{\max}$ , cast film): 3012, 2956, 2931, 2870, 2196, 1633, 1488, 1469, 1463 (sh), 1454, 1416, 1398, 1365, 1277, 1215, 1122, 1077, 991, 961, 853.

**PPE-(4+)**. <sup>1</sup>H NMR (DMSO-*d*<sub>6</sub>; δ ppm): 0.92 (br, 6H), 1.37 (br, 12H), 1.75 (br, 4H), 3.61 (br, 4H), 4.10–4.35 (br, 28H), 4.74 (br, 4H) 7.33–7.86 (aromatic C–H). FTIR ( $\nu_{\max}$ , cast film): 3011, 2956, 2930, 2861, 2205, 1623 (broad), 1518, 1467, 1401, 1281, 1215, 1122, 1073 (sh), 1058, 989, 958, 850, 756, 724, 655, 603, 548.

**PPE-Th-(4+)**. <sup>1</sup>H NMR (DMSO-*d*<sub>6</sub>; δ ppm): 0.90 (br, 6H), 1.35 (br, 12H), 1.76 (br, 4H), 3.61 (br, 4H), 4.04–4.26 (br, 28H),

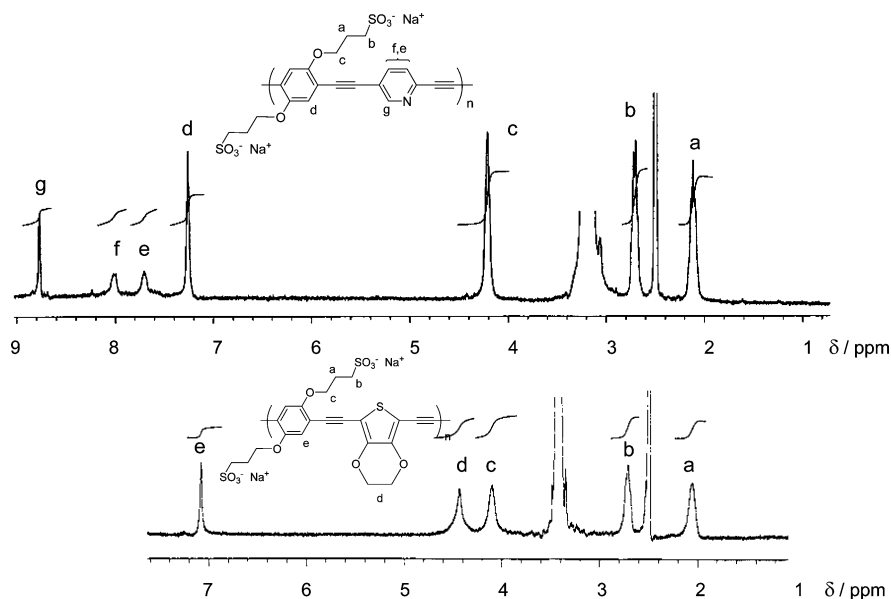
4.73 (br, 4H), 7.39–7.84 (aromatic C–H). FTIR ( $\nu_{\max}$ , KBr pellet): 3006, 2955, 2930, 2869, 2192, 1631, 1621 (sh), 1530, 1494, 1463, 1455 (sh), 1397, 1278, 1214, 1118, 1057, 992, 959, 851, 819, 720, 619.

**PPE-Py-(4+)**. <sup>1</sup>H NMR (DMSO-*d*<sub>6</sub>; δ ppm): 0.90 (br, 6H), 1.35 (br, 12H), 1.78 (br, 4H), 3.64 (br, 4H), 4.13–4.32 (br, 28H), 4.77 (br, 4H), 7.56–9.29 (aromatic C–H). FTIR ( $\nu_{\max}$ , KBr pellet): 2953, 2927, 2857, 2207, 1619, 1583 (sh), 1504, 1467, 1384, 1282, 1245, 1216, 1126, 1055, 1025, 958, 850, 759, 734, 636.

**PPE-BTD-(4+)**. <sup>1</sup>H NMR (DMSO-*d*<sub>6</sub>; δ ppm): 0.83 (br, 6H), 1.27 (br, 12H), 1.67 (br, 4H), 3.52 (br, 4H, partially hidden in water peak), 4.0–4.8 (32H), 7.0–8.2 (aromatic C–H). FTIR ( $\nu_{\max}$ , KBr pellet): 2953, 2927, 2861, 2187, 1628 (broad), 1529, 1502, 1465, 1439, 1398, 1317, 1274, 1204, 1121, 1051, 1021, 953, 850, 759, 708, 543.

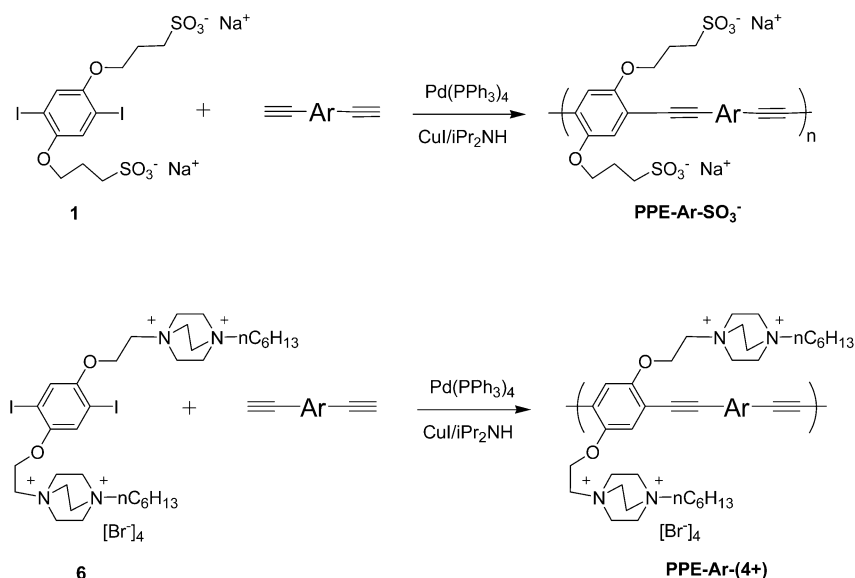
## Results and Discussion

**Structures and Synthesis.** The objective of the present investigation was to synthesize and characterize a series of anionic and cationic PPE-based conjugated polyelectrolytes in which the absorption and fluorescence wavelengths span the visible spectral region. To accomplish this objective, the series of 10 polymers shown in Table 1 were prepared. This series consists of five pairs of polymers that share the same poly(arylene ethynylene) backbone. One member of each pair features anionic R-SO<sub>3</sub><sup>-</sup> side groups, whereas the other member



**Figure 1.**  $^1\text{H}$  NMR spectra of PPE-Py- $\text{SO}_3^-$  (top) and PPE-EDOT- $\text{SO}_3^-$  (bottom) in 0.1 M LiBr/DMSO at 80  $^\circ\text{C}$ . Truncated peaks at  $\approx 2.4$  and 3.3 ppm are DMSO and  $\text{H}_2\text{O}$ , respectively.

**Scheme 1**



contains cationic bis-alkylammonium side groups. The polymers were all synthesized by Pd-mediated coupling reactions between bis-iodo-substituted benzenes that contain the ionic side groups with bis-alkyne-functionalized arenes. In particular, the anionic polymers were prepared by reaction of a bis(dipropylsulfonate) substituted monomer **1** with bis-alkyne-functionalized arenes (Scheme 1). The corresponding cationic polymers were prepared in a similar reaction using the bis(dialkylammonium) substituted monomer **6** in place of **1** (Scheme 1).

The polymerization reactions were carried out in aqueous/DMF solution, and the polymers were purified by repeated precipitation followed by membrane dialysis. Each polymer was characterized by  $^1\text{H}$  NMR spectroscopy; however, it was necessary to develop a special protocol in order to obtain spectra with relatively narrow line widths. In particular, it was found that the NMR line widths were very broad (e.g., 100 Hz or greater) if spectra were obtained at room temperature on polymer samples dissolved in  $\text{D}_2\text{O}$  or  $\text{DMSO}-d_6$ . The line broadening is believed to arise due to the slow rotational correlation time of the polymer chains that is exacerbated by polymer aggregation

(vide infra). NMR spectra with relatively narrow line widths could be obtained by acquisition of the spectra in  $\text{DMSO}-d_6$  solution that contained 0.1 M LiBr. Figure 1 illustrates representative spectra for two of the anionic polymers, PPE-EDOT- $\text{SO}_3^-$  and PPE-Py- $\text{SO}_3^-$ . The spectrum of PPE-EDOT- $\text{SO}_3^-$  exhibits aliphatic resonances characteristic of the 2,5-ethylene(dioxythiophene) unit ( $\delta = 4.44$ ) as well as those arising from the  $-\text{O}-\text{CH}_2\text{CH}_2\text{CH}_2-\text{SO}_3^-$  units ( $\delta = 2.08$ , 2.71, and 4.14) and a single aromatic resonance due to the dialkoxybenzene moiety ( $\delta = 7.08$ ). The spectrum of PPE-Py- $\text{SO}_3^-$  also features the aliphatic resonances due to  $-\text{O}-\text{CH}_2\text{CH}_2\text{CH}_2-\text{SO}_3^-$  as well as three aromatic resonances due to the 2,5-pyridyl (Py) unit ( $\delta = 7.71$ , 7.99, and 8.77), along with a single peak due to the dialkoxybenzene ( $\delta = 7.26$ ). In both cases, despite the elevated temperature and addition of salt, the spectra still display relatively broad line widths. This situation is most pronounced for PPE-EDOT- $\text{SO}_3^-$ , where the broadening makes it difficult to discern the splitting due to proton-proton coupling for the protons in the  $-\text{O}-\text{CH}_2\text{CH}_2\text{CH}_2-\text{SO}_3^-$  units. For all of the polymers, there was no evidence of resonances arising



Table 2. Photophysical and Fluorescence Quenching Data for Conjugated Polyelectrolytes

polymer <sup>a</sup>	solvent	$\lambda_{\max}^{\text{abs}}/\text{nm}$	$\lambda_{\max}^{\text{fl}}/\text{nm}$	$\phi_{\text{fl}}$	$\tau_{\text{fl}}/\text{ns}$	$K_{\text{SV}}/\mu\text{M}^{-1}$	$[\text{Q}]_{90}/\mu\text{M}$
PPE-SO <sub>3</sub> <sup>-</sup>	MeOH	425	447	0.78 <sup>d</sup>	450 nm: 0.42 (97%), 1.60 (3%)	7, SL	0.66
	H <sub>2</sub> O	446	547	0.10 <sup>d</sup>	450 nm: 0.55 (44%), 5.28 (56%)	8.9, SL	0.50
PPE-Py-SO <sub>3</sub> <sup>-</sup>	MeOH	432	457	0.303 <sup>e</sup>	450 nm: 0.6 (94%), 3 (6%)	1.77	
	H <sub>2</sub> O	455	532	0.187 <sup>e</sup>	550 nm: 2.83 (62%), 7.62 (38%)	11.8, SL	1.0
PPE-Th-SO <sub>3</sub> <sup>-</sup>	MeOH	454	480	0.265 <sup>e</sup>	500 nm: 0.3 (95%), 3.2 (5%)	2.38, SL	1.33
	H <sub>2</sub> O	484	478	0.036 <sup>e</sup>	500 nm: 0.1 (73%), 2.5 (27%)	2.2	>5
PPE-EDOT-SO <sub>3</sub> <sup>-</sup>	MeOH	493	496	0.019 <sup>f</sup>	500 nm: 0.6 (93%), 3.8 (7%)	1.65, SL	1.65
	H <sub>2</sub> O	506	c	c	c	1.80	>5
PPE-BTD-SO <sub>3</sub> <sup>-</sup>	MeOH	514	592	0.03 <sup>g</sup>	600 nm: 0.74 (89%), 3.41 (11%)	1.43	
	H <sub>2</sub> O	549	634	0.00034 <sup>g</sup>	c	c	
PPE-(4+)	MeOH	422	441	0.15 <sup>h</sup>	450 nm: 0.13 (93%), 0.78 (7%)	1.76	
	H <sub>2</sub> O	394	436	0.047 <sup>h</sup>	450 nm: 0.88 (84%), 3.19 (16%)	1.46	
PPE-Py-(4+) <sup>b</sup>	MeOH	424	450	0.047 <sup>e</sup>	450 nm: 0.5 (97%), 3.8 (3%)	0.24	
	H <sub>2</sub> O	426	508	0.008 <sup>e</sup>	450 nm: 0.3 (95%), 2.8 (5%)	0.24	
PPE-Th-(4+)	MeOH	447	482	0.14 <sup>e</sup>	475 nm: 0.34 (100%)	0.74	
	H <sub>2</sub> O	429	478	0.071 <sup>e</sup>	475 nm: 0.15 (100%)	0.74	
PPE-EDOT-(4+)	MeOH	475	504	0.060 <sup>f</sup>	500 nm: 0.20 (94%), 1.1 (5%)	1.20	
	H <sub>2</sub> O	455	496	0.011 <sup>f</sup>	550 nm: 0.83 (88%), 3.46 (12%)	1.65	
PPE-BTD-(4+)	MeOH	511	603	0.011 <sup>f</sup>	600 nm: 0.53 (88%), 4.07 (12%)	0.422	
	H <sub>2</sub> O	520	630	0.0006 <sup>f</sup>	c	c	

<sup>a</sup> 10  $\mu\text{M}$ . <sup>b</sup> In 0.1 mM NaOH. <sup>c</sup> Fluorescence too weak. <sup>d</sup> Fluorescein in EtOH as standard,  $\phi_{\text{fl}} = 0.79$ , see ref 52. <sup>e</sup> Coumarin 6 in EtOH as standard,  $\phi_{\text{fl}} = 0.78$ , see ref 53. <sup>f</sup> Rhodamine 6G in EtOH as standard,  $\phi_{\text{fl}} = 0.95$ , see ref 54. <sup>g</sup> Crystal violet perchlorate in EtOH as standard,  $\phi_{\text{fl}} = 0.54$ , see ref 55. <sup>h</sup> Coumarin 1 in EtOH as standard,  $\phi_{\text{fl}} = 0.73$ , see ref 56.

from polymer end groups (e.g., protons on an aryl halide unit or terminal acetylene protons). The absence of peaks due to end groups makes it possible to conservatively estimate that a lower limit for the degree of polymerization for each polymer is  $X_n \geq 10$ .

Unfortunately, it was not possible to apply GPC to obtain direct information regarding molecular weight and polydispersity for the CPEs. In the absence of these data, all of the polymers were characterized by viscometry in order to obtain an indication of the relative chain lengths. For each polymer, the intrinsic viscosity ( $[\eta]$ ) was determined by measuring the specific viscosity ( $\eta_{\text{sp}}$ ) for the polymers at four different concentrations in 0.1 M LiBr/DMSO solution and extrapolating the linear plot of  $\eta_{\text{sp}}/c$  vs  $c$  to infinite dilution.<sup>26</sup>

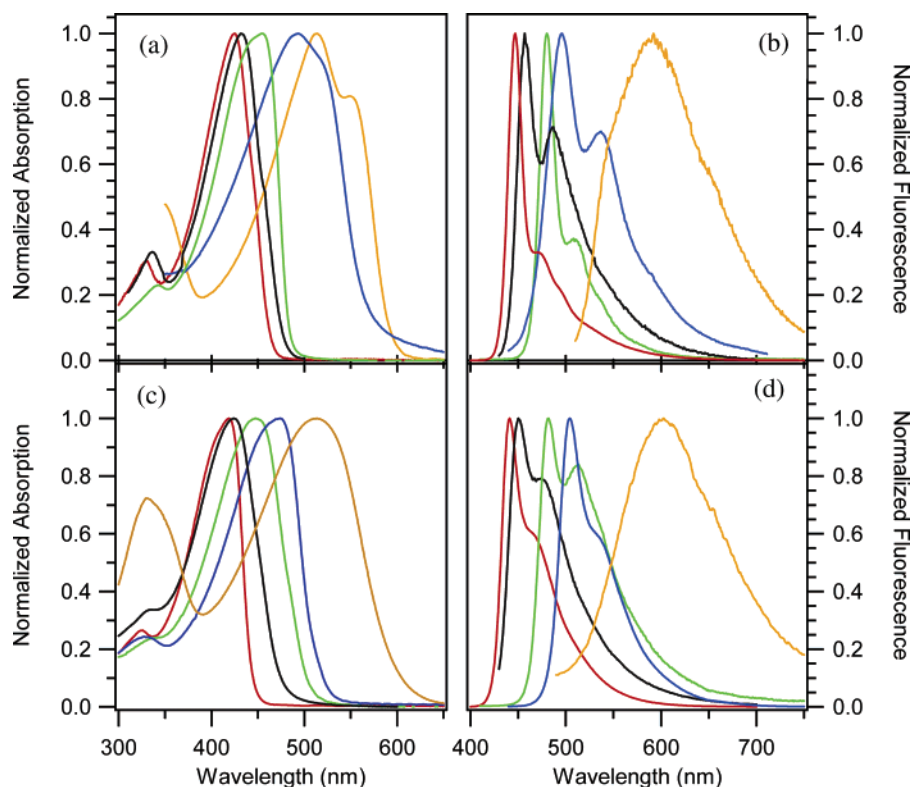
Table 1 contains a listing of the intrinsic viscosity for the 10 polymers, and several trends can be seen in the data. First, in general, the  $[\eta]$  values for the PPE-Ar-SO<sub>3</sub><sup>-</sup> series are larger compared to those for the PPE-Ar-(4+) series, suggesting that the former (anionic) polymers generally have higher chain lengths. This finding suggests that the sulfonate-substituted monomer **1** is more reactive with respect to polymerization compared to the tetralkylammonium monomer **6**. The lower reactivity of the latter monomer may be the result of a steric effect of the bulky diazabicyclooctane (DABCO) based alkylammonium groups. Second, the  $[\eta]$  values for the phenylene-based polymers PPE-SO<sub>3</sub><sup>-</sup> and PPE-(4+) are noticeably larger than those for the polymers that contain the heterocyclic rings. Although this result suggests that these polymers have a comparatively larger degree of polymerization, note that the polymers that contain the thienyl groups will have less rigid-rod character, which may result in these materials having lower intrinsic viscosity for a similar degree of polymerization. In any event, on the basis of the <sup>1</sup>H NMR and viscometry results, we conclude that all of the CPEs exist as polymers with moderate degrees of polymerization (likely ranging from  $10 < X_n < 100$ ), where the higher chain lengths are for the phenylene-based polymers (PPE-SO<sub>3</sub><sup>-</sup> and PPE-(4+)) and the lower chain lengths are for the PPE-Ar-(4+) with Th and BTD arylene units.

**Absorption and Fluorescence Properties.** A comprehensive study was carried out in which the absorption and fluorescence spectra of the 10 CPEs were measured in MeOH, H<sub>2</sub>O, and in

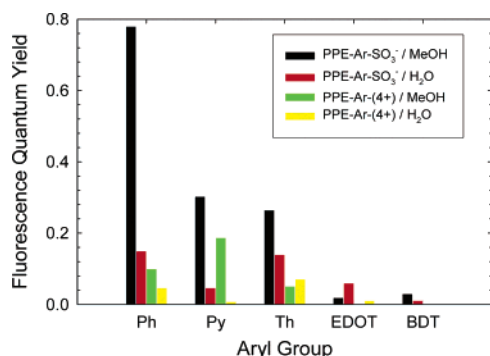
mixtures of the two solvents. This pair of solvents was selected on the basis of previous work on PPE-SO<sub>3</sub><sup>-</sup>, which indicates that, for these PPE-type CPEs, MeOH is a “good solvent” (i.e., the polymers exist in a “molecularly dissolved” state with minimal aggregation) and H<sub>2</sub>O is a “poor solvent” (i.e., the polymers exist as aggregates).<sup>5,15</sup> Table 2 compiles the optical data, including a listing of the absorption and fluorescence maxima ( $\lambda_{\max}^{\text{abs}}$  and  $\lambda_{\max}^{\text{fl}}$ , respectively).

Figure 2 illustrates the complete set of absorption and fluorescence spectra of the ten CPEs in MeOH. In general, there is a close correspondence between the wavelength maxima and band shape for the corresponding pairs of anionic and cationic PPE-type CPEs. This is not surprising in view of the fact that the polymers’ optical properties are mainly determined by the structure of the  $\pi$ -conjugated backbone. In addition, the absorption and emission spectra of the various CPEs correspond closely with the previously reported spectra of structurally analogous polymers that contain alkyl- or alkoxy-solubilizing groups (measured in organic solvents).<sup>20,27</sup>

In both the PPE-Ar-SO<sub>3</sub><sup>-</sup> and PPE-Ar-(4+) series, the wavelength maxima of the absorption, and fluorescence spectra systematically red-shift in the order phenyl < Py < Th < EDOT < BTD. Across the entire series, the absorption maximum shifts from ca. 410 nm (PPE-SO<sub>3</sub><sup>-</sup> and PPE-(4+)) to 520 nm (PPE-BDT-SO<sub>3</sub><sup>-</sup> and PPE-BDT-(4+)), whereas the fluorescence maxima shift from ca. 440 nm (PPE-SO<sub>3</sub><sup>-</sup> and PPE-(4+)) to 600 nm (PPE-BDT-SO<sub>3</sub><sup>-</sup> and PPE-BDT-(4+)). The origin of the red-shifts in the absorption and fluorescence likely arise from several factors that vary with the structure of the heterocycle in the PAE backbone. Specifically, the red-shift for the 2,5-thienyl (Th) and 3,4-ethylenedioxy-2,5-thienyl (EDOT) polymers likely arises because the HOMO level of the polymer is increased because of the electron-donor characteristic of the Th and EDOT units.<sup>28</sup> The increase in the HOMO energy reduces the HOMO–LUMO gap, thereby reducing the energy of the lowest singlet excited state. In contrast to the Th and EDOT polymers, in the 2,5-pyridyl (Py) and 2,1,3-benzothiadiazole (BDT) polymers the nitrogen-containing heterocycles likely act as electron acceptors, thereby reducing the LUMO level of the polymer.<sup>29</sup> In effect, in these polymers, the dialkoxybenzene repeat acts as a donor and the Py or BDT



**Figure 2.** Normalized absorption (a) and fluorescence (b) of PPE-SO<sub>3</sub><sup>−</sup> (red solid lines), PPE-Py-SO<sub>3</sub><sup>−</sup> (black solid lines), PPE-Th-SO<sub>3</sub><sup>−</sup> (green solid lines), PPE-EDOT-SO<sub>3</sub><sup>−</sup> (blue solid lines), and PPE-BTD-SO<sub>3</sub><sup>−</sup> (yellow solid lines) in methanol solution. Normalized absorption (c) and fluorescence (d) of PPE-(4+) (red solid lines), PPE-Py-(4+) (black solid lines), PPE-Th-(4+) (green solid lines), PPE-EDOT-(4+) (blue solid lines), and PPE-BTD-(4+) (yellow solid lines) in methanol solution.



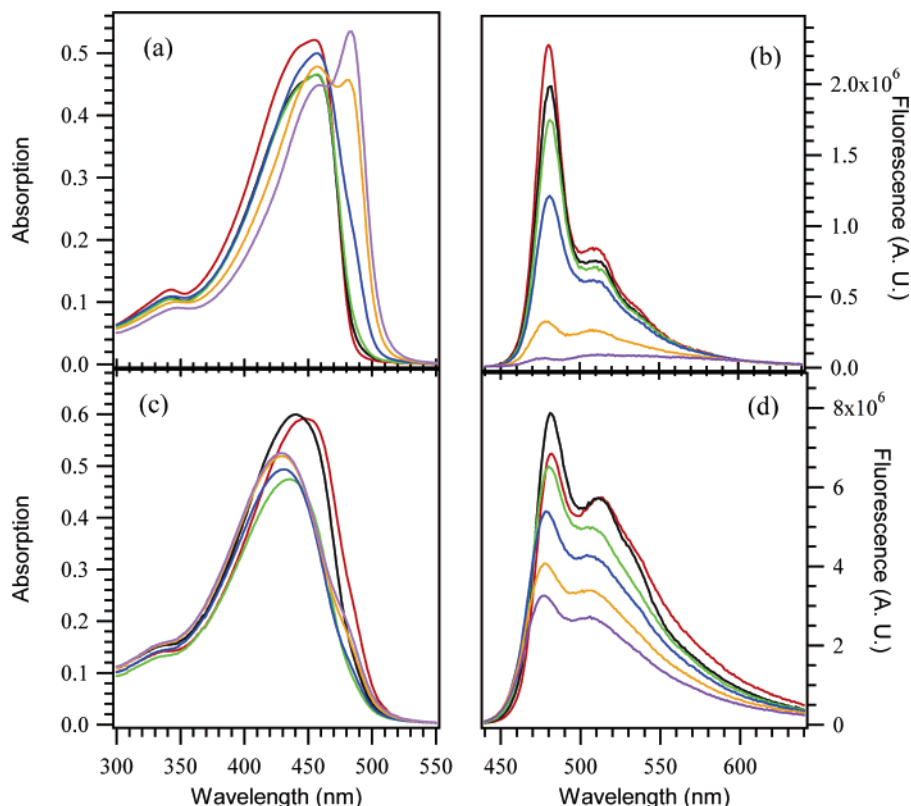
**Figure 3.** Plot of fluorescence quantum yields for CPEs in water and methanol. Black: PPE-Ar-SO<sub>3</sub><sup>−</sup> in methanol. Red: PPE-Ar-SO<sub>3</sub><sup>−</sup> in water. Green: PPE-Ar-(4+) in methanol. Yellow: PPE-Ar-(4+) in water.

groups act as electron acceptors, giving rise to charge-transfer character in the lowest excited state. The existence of charge-transfer character in the singlet state of PPE-BTD-SO<sub>3</sub><sup>−</sup> and PPE-BTD-(4+) polymers is evidenced by the relatively large Stokes shift (ca. 85 nm) combined with the broad, structureless band shape of the fluorescence spectra.

To gain more insight into the photophysical properties of the polymers, the fluorescence quantum yields ( $\phi_f$ ) and fluorescence decay kinetics were measured. The numerical values are tabulated in Table 2, and the  $\phi_f$  values in MeOH and H<sub>2</sub>O are presented as a bar graph in Figure 3. Several trends are evident in the  $\phi_f$  data. First, in general the yields are largest for the PPE-Ar-SO<sub>3</sub><sup>−</sup> series in MeOH; for most of the corresponding pairs of anionic and cationic polymers, the yields are lower for the PPE-(4+) series in MeOH. The origin of this effect is unclear, but one possibility is that the lower  $\phi_f$  values for the PPE-(4+) series arise due to their relatively shorter chain

lengths. Second, across the PPE-Ar-SO<sub>3</sub><sup>−</sup> series, the  $\phi_f$  values systematically decrease in the sequence Ph > Py > Th > BDT > EDOT. Interestingly, this ordering correlates approximately with the emission energy, i.e.,  $\phi_f$  generally decreases with decreasing emission energy. This effect is consistent with the increased charge-transfer character inherent in the excited states of the polymers that fluoresce at longer wavelengths. Increased charge-transfer character leads to localization of the exciton, with a concomitant decrease in the radiative decay rate.<sup>30</sup> Regardless of the origin of the effect, it is clear that the polymers that fluoresce at longer wavelength (i.e., Ar = EDOT and BDT) do so with considerably lower efficiency compared to the blue-emitting polymers (i.e., Ar = Ph and Py). This result is unfortunate for possible applications of the PPE-based CPEs (e.g., as fluorescence sensors) where efficient long wavelength fluorescence is a desirable characteristic. The third effect that is clearly evident is that the  $\phi_f$  values are dramatically lower for all of the polymers in H<sub>2</sub>O solution. This effect has been previously observed for PPE-SO<sub>3</sub><sup>−</sup><sup>5,15</sup> and has been attributed to aggregation-induced quenching of the intrachain singlet exciton. The effect of solvent-induced aggregation is explored more fully below, where studies of the effect of solvent on the absorption and fluorescence are described.

The fluorescence decay kinetics for the polymers were measured at wavelengths corresponding closely to the fluorescence maximum. In MeOH solution, in each case, the decays are characterized by a large-amplitude, short-lifetime decay component (e.g., >90%,  $\tau$  < 0.5 ns), and a low-amplitude component (<10%) with a lifetime of several nanoseconds. The decay kinetics are more complicated for the polymers in H<sub>2</sub>O solution. First, for the polymers that remain reasonably strongly fluorescent in H<sub>2</sub>O, overall the fluorescence decays more slowly than it does in MeOH. For example, for PPE-SO<sub>3</sub><sup>−</sup>, PPE-Py-



**Figure 4.** (a) Absorption of PPE-Th-SO<sub>3</sub><sup>-</sup>; (b) fluorescence of PPE-Th-SO<sub>3</sub><sup>-</sup>; (c) absorption of PPE-Th-(4+); (d) fluorescence of PPE-Th-(4+). Red solid lines: 0% H<sub>2</sub>O; black solid lines: 20% H<sub>2</sub>O; green solid lines: 40% H<sub>2</sub>O; blue solid lines: 60% H<sub>2</sub>O; yellow solid lines: 80% H<sub>2</sub>O; violet solid lines: 100% H<sub>2</sub>O.

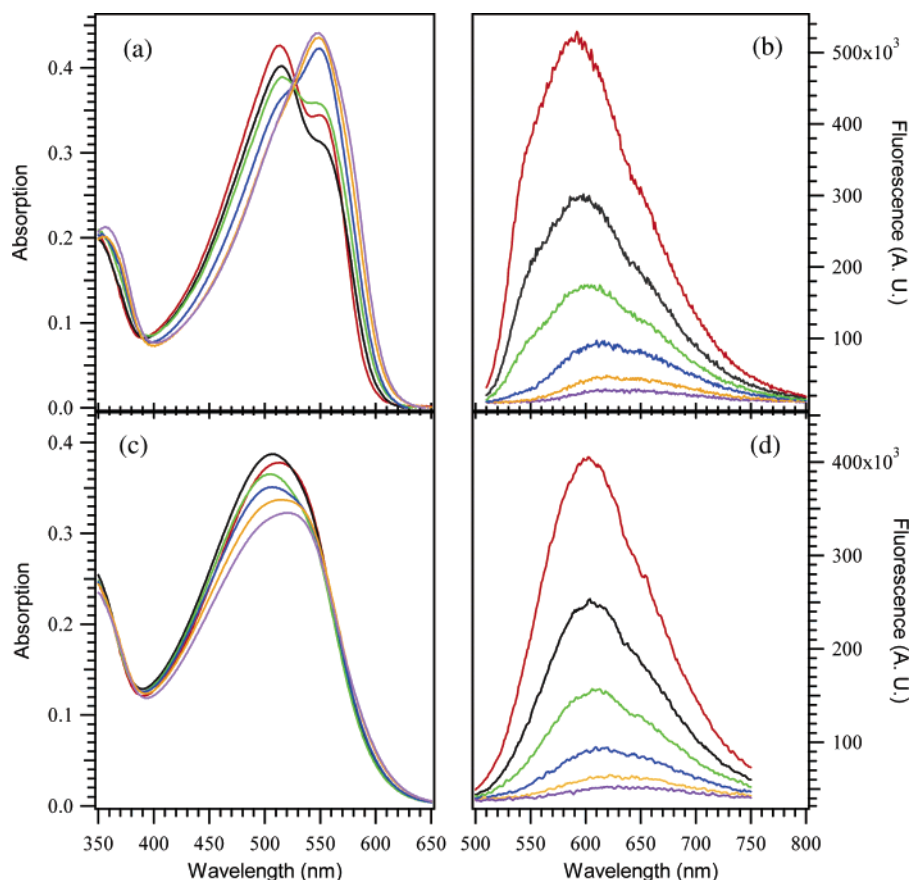
SO<sub>3</sub><sup>-</sup>, and PPE-(4+) in water, the decays consist of two components with significant amplitude, one having a lifetime of 1 ns or less, and a second with a lifetime in excess of 3 ns. This behavior is consistent with the fluorescence emanating from an “excimer-like” state, which has a decreased radiative decay rate compared to an intrachain singlet exciton.<sup>31</sup> By contrast, for those polymers that display strong fluorescence quenching in H<sub>2</sub>O, the fluorescence decays more rapidly compared to the kinetics in MeOH. This behavior is typified by PPE-Th-SO<sub>3</sub><sup>-</sup> and PPE-Th-(4+); for both of these polymers, the fluorescence decays in water are dominated by a very short-lived decay component ( $\tau < 300$  ps). This behavior is consistent with the presence of a nonfluorescent (or very weakly fluorescent) aggregate state for these polymers in water. The aggregate state apparently acts as a trap, leading to rapid quenching of the intrachain exciton.

**Solvent Effects on Absorption and Fluorescence: CPE Aggregation in Water.** In several previous investigations of PPE-SO<sub>3</sub><sup>-</sup>, we have shown that this polymer has a strong tendency to aggregate in aqueous solution.<sup>5,15</sup> Chain aggregation is signaled by a red-shift and narrowing of the polymer’s absorption spectrum, a significant red-shift and broadening of the fluorescence spectrum, and a decrease in  $\phi_f$ . On the basis of this previous work, we anticipated that the series of variable band gap PAEs that are the subject of this investigation would also aggregate in aqueous solution. To explore this effect, and how it influences the optical properties of the new polymers, a series of experiments were carried out in which the absorption and fluorescence spectra of all of the CPEs were studied in MeOH/H<sub>2</sub>O mixtures of varying composition.

In general, the studies of the solvent dependence on the absorption and fluorescence properties clearly indicate that all of the CPEs undergo interchain aggregation as the volume

fraction of H<sub>2</sub>O in the solvent increases. However, an interesting observation is that the effect of aggregation on the optical properties of the PPE-Ar-(4+) series is attenuated compared to its effect on the PPE-Ar-SO<sub>3</sub><sup>-</sup> series. Although there are quantitative differences among properties of the individual polymers, the effect of solvent on the fluorescence within the PPE-Ar-SO<sub>3</sub><sup>-</sup> series and within the PPE-Ar-(4+) series is generally similar, and therefore, we only present representative sets of data for the polymers with Ar = Th and BTd.

Figure 4 illustrates the fluorescence and absorption spectra of PPE-Th-SO<sub>3</sub><sup>-</sup> and PPE-Th-(4+) in MeOH/H<sub>2</sub>O mixtures. For the anionic polymer (PPE-Th-SO<sub>3</sub><sup>-</sup>, Figure 4a) the absorption undergoes a very clear red-shift and narrowing as the volume fraction of H<sub>2</sub>O increases. Interestingly, the series of absorption spectra approximately define an isosbestic point at 470 nm, suggesting that the solvent-induced change is between two distinct types of chromophores. The fluorescence of PPE-Th-SO<sub>3</sub><sup>-</sup> (Figure 4b) decreases significantly in intensity (quantum efficiency) as the volume fraction of H<sub>2</sub>O increases. In pure H<sub>2</sub>O, the emission is very weak, and the spectrum of the residual weak fluorescence that is observed is enhanced on the red side of the band. As seen in parts c and d of Figure 4, the effect of solvent on the absorption and fluorescence of PPE-Th-(4+) is muted when compared to the changes seen for PPE-Th-SO<sub>3</sub><sup>-</sup>. In particular, in all of the solvent mixtures, the absorption is comparatively broad and there is only a slight blue-shift in the absorption as the volume fraction of H<sub>2</sub>O increases. The fluorescence intensity of PPE-Th-(4+) increases slightly as the solvent is changed from 100% to 80% MeOH, but then it systematically decreases with increasing volume fraction of H<sub>2</sub>O. However, note that the fluorescence quantum yield in pure H<sub>2</sub>O is only 50% less than that in pure MeOH, and the



**Figure 5.** (a) Absorption of PPE-BTD-SO<sub>3</sub><sup>−</sup>; (b) fluorescence of PPE-BTD-SO<sub>3</sub><sup>−</sup>; (c) absorption of PPE-BTD-(4+); (d) fluorescence of PPE-BTD-(4+). Red solid lines: 0% H<sub>2</sub>O; black solid lines: 20% H<sub>2</sub>O; green solid lines: 40% H<sub>2</sub>O; blue solid lines: 60% H<sub>2</sub>O; yellow solid lines: 80% H<sub>2</sub>O; violet solid lines: 100% H<sub>2</sub>O.

fluorescence of the polymer remains relatively efficient even in water.

A very similar pattern emerges when comparing the solvent effects on the absorption and fluorescence of PPE-BTD-SO<sub>3</sub><sup>−</sup> and PPE-BTD-(4+), Figure 5. First, as shown in Figure 5a, the absorption spectrum of the anionic polymer undergoes a 34 nm red-shift with increasing volume fraction of H<sub>2</sub>O. The series of absorption spectra obtained in the series of MeOH/H<sub>2</sub>O mixtures features an isosbestic point at 535 nm, again suggesting that the solvent induces a change between two distinct chromophoric states of the polymer. The fluorescence of PPE-BTD-SO<sub>3</sub><sup>−</sup> (Figure 5b) decreases significantly in intensity and red-shifts 42 nm with increasing volume fraction H<sub>2</sub>O. In pure water, the emission is weak, exhibiting  $\phi_f = 3 \times 10^{-4}$ . The solvent-induced changes in the absorption and fluorescence of the cationic polymer, PPE-BTD-(4+), are again less pronounced compared to those of the anionic counterpart. In particular, the absorption spectrum undergoes a slight red-shift (ca. 9 nm) with increasing volume fraction of H<sub>2</sub>O. The fluorescence is quenched in this polymer with increasing volume fraction H<sub>2</sub>O, however, the red-shift is less significant than that seen for PPE-BTD-SO<sub>3</sub><sup>−</sup>.

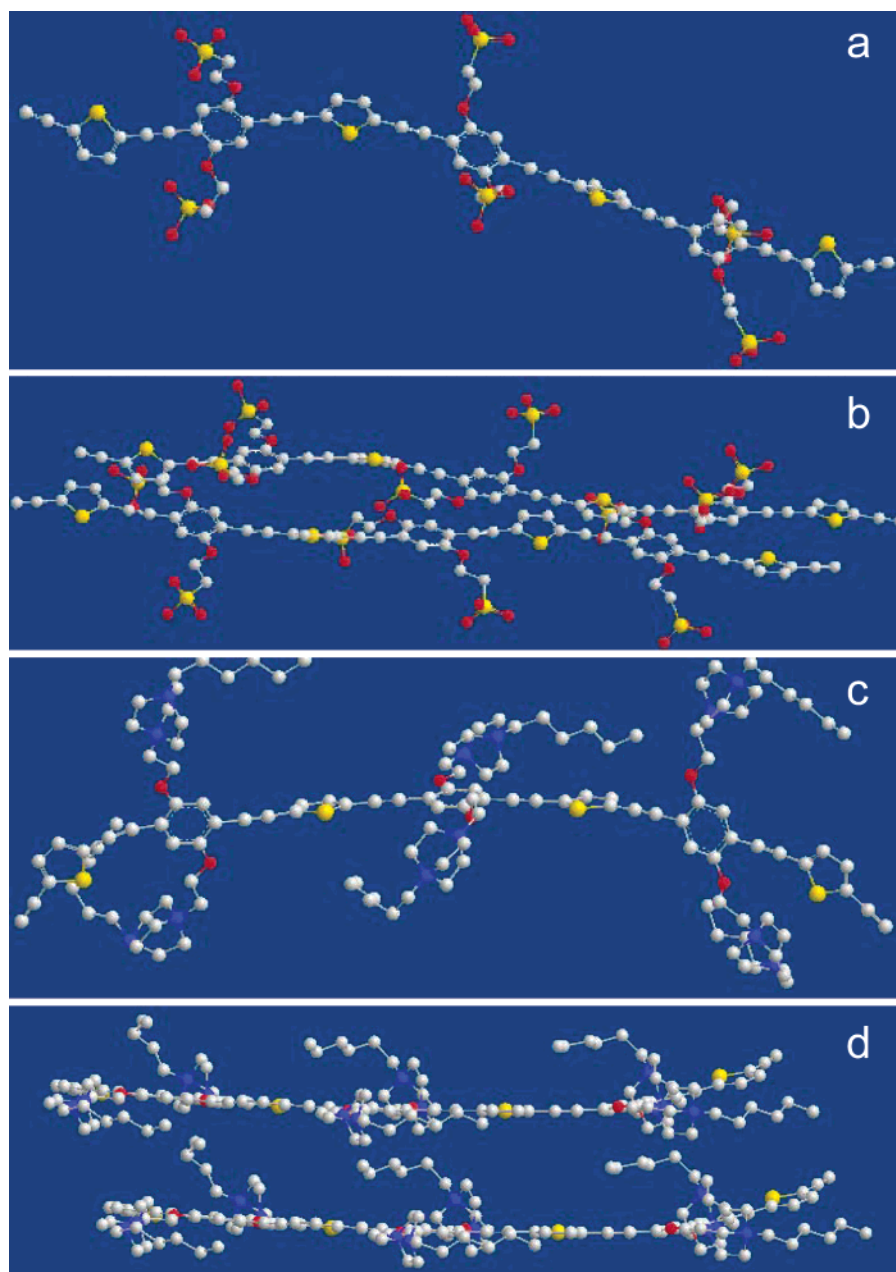
The explanation for the solvent effect on the absorption and fluorescence properties of the series of variable band gap CPEs is similar to the one used to explain similar effects on the parent polymer, PPE-SO<sub>3</sub><sup>−</sup>.<sup>5,15</sup> In particular, it is believed that both the anionic (PPE-Ar-SO<sub>3</sub><sup>−</sup>) and cationic (PPE-Ar-(4+)) polymers exist as molecularly dissolved chains in MeOH solution, but in H<sub>2</sub>O solution, the polymers aggregate due to their amphiphilic character. Interchain aggregation is mainly driven by the hydrophobic effect, coupled with a weak favorable

enthalpy for  $\pi$ -stacking interactions between adjacent aryl residues in the chains.

The pronounced spectral changes observed for the PPE-Ar-SO<sub>3</sub><sup>−</sup> series accompanying chain aggregation are explained as follows. In MeOH, the chains are well-solvated, and consequently, interchain interactions are minimal. Because of the low barrier for bond rotation around the Ar-C $\equiv$ C-Ar unit, the aryl groups take on a random distribution of conformations along the backbone.<sup>32</sup> This effect is clearly seen in the MM2 minimized structure of a PPE-Th-SO<sub>3</sub><sup>−</sup> segment shown in Figure 6a. Because of the random conformation of the aryl units, there is a broad distribution of segments that differ in the extent of  $\pi$ -conjugation along the backbone. This gives rise to the relatively broad and blue-shifted absorption band observed in MeOH. We posit that, in H<sub>2</sub>O solution, the aggregated PPE-Ar-SO<sub>3</sub><sup>−</sup> chains stack so as to optimize interchain  $\pi$ - $\pi$  interactions. As shown by the model in Figure 6b for a pair of PPE-Th-SO<sub>3</sub><sup>−</sup> segments, interchain stacking arranges the aryl groups so that they are optimized for  $\pi$ -conjugation along the polymer backbone. This leads to the red-shift and narrowing of the absorption band.<sup>33–35</sup> The fluorescence quenching arises due to interchain  $\pi$ - $\pi$  interactions. In particular, for the PPE-Th-SO<sub>3</sub><sup>−</sup> and PPE-BTD-SO<sub>3</sub><sup>−</sup>, the interchain excited-state interaction likely has significant charge-transfer character (i.e., by analogy to an "exciplex").<sup>31,36</sup> The charge-transfer character in the excited state leads to pathways for rapid nonradiative decay, which result in fluorescence quenching.

Although the optical data suggest that PPE-Th-(4+) and PPE-BTD-(4+) aggregate in H<sub>2</sub>O solution, it is important to understand why the absorption and fluorescence change less for these polymers as the solvent is changed from MeOH to



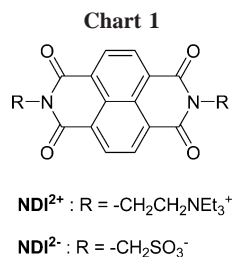


**Figure 6.** Molecular models of 3 repeat unit segments (6 arylene ethynylenes) generated by using MM2 molecular mechanics in Chem3D Pro (version 9.0). Hydrogen atoms omitted for clarity. (a) PPE-Th-SO<sub>3</sub><sup>−</sup> energy minimized structure of a single chain. (b) PPE-Th-SO<sub>3</sub><sup>−</sup> energy minimized structure of two stacked chains. Note that the two conjugated backbones can come into close proximity. (c) PPE-Th-(4<sup>+</sup>) energy minimized structure of a single chain. (d) PPE-Th-(4<sup>+</sup>) energy minimized structure of two stacked chains. Note that the side chains prevent the conjugated backbones from coming into close proximity.

H<sub>2</sub>O. We believe that the difference arises because the bulky ammonium side groups in the PPE-Ar-(4<sup>+</sup>) polymers prevent the  $\pi$ -conjugated segments from coming into close proximity in the polymer aggregates. In particular, as illustrated by Figure 6c, in isolated PPE-Th-(4<sup>+</sup>) chains, the  $\pi$ -conjugated backbone takes on a random conformation; thus, in MeOH, PPE-Th-(4<sup>+</sup>) is similar to its anionic counterpart, PPE-Th-SO<sub>3</sub><sup>−</sup>. However, when PPE-Th-(4<sup>+</sup>) aggregates due to strong steric interactions between the bulky diazabicyclo[2.2.2]octane (DABCO) based side-groups, it is not possible for the chains to pack in such a way so as to induce the aromatic rings to take on the “all-planar” conformation that is responsible for the changes in the optical spectra. This effect is nicely illustrated by the molecular simulation in Figure 6d that shows stacked PPE-Th-(4<sup>+</sup>) chains. It is quite evident from the simulation that the DABCO-based sidegroups present a steric barrier that precludes

the  $\pi$ -conjugated backbone of two chains from coming into close proximity. Nevertheless, as evidenced by the reduced  $\phi_{\text{fl}}$  for PPE-Th-(4<sup>+</sup>) and PPE-BTD-(4<sup>+</sup>) in H<sub>2</sub>O compared to MeOH, there clearly remain some interchain electronic interactions in the PPP-Ar-(4<sup>+</sup>) aggregates. However, the interactions are less, which gives rise to the smaller solvent-induced changes seen for the cationic polymers.

**Amplified Fluorescence Quenching.** As noted above, much of the interest in CPEs has arisen due to their fluorescence-quenching properties.<sup>4,13,14,37–42</sup> In particular, it has been shown that the fluorescence of anionic-conjugated polyelectrolytes is quenched by very low concentrations of cationic quenchers<sup>4,5,12,14,15,40,43</sup> and that the fluorescence of cationic CPEs is quenched by low concentrations of anionic quenchers.<sup>6,9,13,41,44</sup> Recent studies by our group, and others, have also shown that the sensitivity of the quenching response (as reflected by the



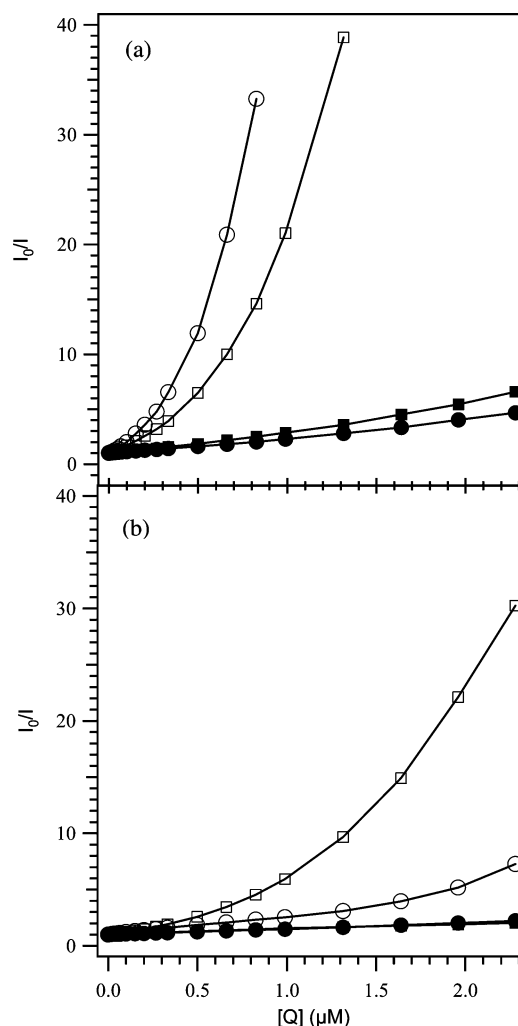
Stern–Volmer quenching constant,  $K_{\text{SV}}$ ) is enhanced by aggregation of the CPE chains.<sup>4,14,15,40</sup>

To examine how the amplified fluorescence-quenching effect depends on CPE structure and charge type, in the course of the present study, the fluorescence-quenching response of the five pairs of anionic and cationic CPEs was examined. The pair of oppositely charged naphthalene diimides shown in Chart 1 were used as quenchers. The naphthalene diimide electrophore is reduced at a relatively low potential,  $E_{1/2} \approx -0.53$  V vs SCE,<sup>45</sup> and therefore it is believed to quench the CPE fluorescence via a charge-transfer mechanism (where the excited-state CPE is the donor). Stern–Volmer (SV) quenching plots were generated for each polymer from quenching studies carried out in MeOH and H<sub>2</sub>O; the cationic quencher ( $\text{NDI}^{2+}$ ) was used with the anionic PPE-Ar- $\text{SO}_3^-$  series, whereas the anionic quencher ( $\text{NDI}^{2-}$ ) was used with the cationic PPE-Ar-(4+) series. (Quenching was very inefficient with quencher/polymer pairs  $\text{NDI}^{2+}/\text{PPE-Ar-(4+)}$  or  $\text{NDI}^{2-}/\text{PPE-Ar-SO}_3^-$ .) Some of the SV plots are superlinear (i.e., they display upward curvature), and in these cases, the plots are characterized by a  $K_{\text{SV}}$  value obtained from the linear portion of the curve at low quencher concentration, along with the  $[\text{Q}]_{90}$  value, which is defined as the quencher concentration that affords 90% fluorescence quenching.

Fluorescence-quenching data for the 10 CPEs is summarized in Table 2, and representative SV quenching plots for two pairs of polymers in MeOH and H<sub>2</sub>O are shown in Figure 7. Close inspection of these data reveals several significant trends. First, it is evident that fluorescence quenching is generally more efficient for the PPE-Ar- $\text{SO}_3^-$  series than for the PPE-Ar-(4+) polymers. This trend is clear from the SV plots shown in Figure 7, where PPE- $\text{SO}_3^-$  and PPE-Th- $\text{SO}_3^-$  exhibit much stronger quenching when compared with the plots for PPE-(4+) and PPE-Th-(4+). Second, four of the five PPE-Ar- $\text{SO}_3^-$  series exhibit superlinear SV plots, whereas all of the SV plots for the PPE-Ar-(4+) series exhibit relatively linear SV plots.

While the quenching efficiency varies more than 20-fold across the series of CPEs, in every case, quenching is relatively efficient: the smallest  $K_{\text{SV}}$  value observed is  $2.4 \times 10^5 \text{ M}^{-1}$  (for  $\text{NDI}^{2-}$  quenching of PPE-Py-(4+)). Quenching was not observed when similarly charged polymers and quenchers were mixed, a finding which indicates that, for all of the CPEs, fluorescence-quenching occurs by a “static quenching” mechanism involving an ion-pair complex between the oppositely charged CPE chain and the quencher.<sup>4,15,46</sup> In addition, the quenching efficiencies for all of the polymers are more than an order of magnitude larger than for static quenching of an ionic fluorescent small molecule by an oppositely charged quencher.<sup>12</sup> Thus, for all of the CPEs, “amplified quenching” occurs; however, the extent by which the quenching is amplified varies significantly across the series.

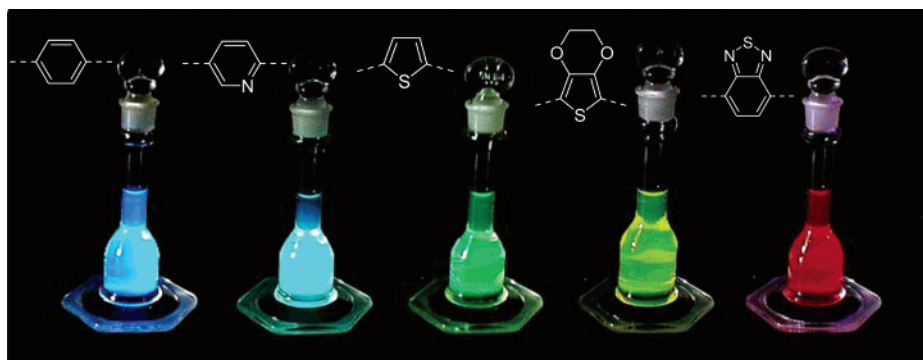
We believe that the difference in the quenching efficiency across the series of CPEs arises due to the difference in aggregation behavior of the PPE-Ar- $\text{SO}_3^-$  and PPE-Ar-(4+)



**Figure 7.** (a)  $\circ$ : PPE- $\text{SO}_3^-$  in H<sub>2</sub>O;  $\square$ : PPE- $\text{SO}_3^-$  in CH<sub>3</sub>OH;  $\bullet$ : PPE-(4+) in H<sub>2</sub>O;  $\blacksquare$ : PPE-(4+) in CH<sub>3</sub>OH. (b)  $\circ$ : PPE-Th- $\text{SO}_3^-$  in H<sub>2</sub>O;  $\square$ : PPE-Th- $\text{SO}_3^-$  in CH<sub>3</sub>OH;  $\bullet$ : PPE-Th-(4+) in H<sub>2</sub>O;  $\blacksquare$ : PPE-Th-(4+) in CH<sub>3</sub>OH.

chains. In previous investigations, it has been shown that the quenching efficiency of CPEs by oppositely charged quenchers is most efficient when the polymer chains are strongly aggregated (i.e., there are strong  $\pi$ - $\pi$  interchain interactions, as illustrated in Figure 6b).<sup>4,14,15,40</sup> This effect is believed to arise because, in the aggregate, the fluorescent (singlet) exciton is able to undergo rapid inter- and intrachain migration, effectively allowing a single quencher ion to quench excitons produced on many chains.<sup>4,15,47</sup> This effect is believed to be the reason why members of the PPE-(4+) series are quenched less efficiently compared to those in the PPE-Ar- $\text{SO}_3^-$  series. In particular, as discussed above, because of the bulky DABCO-based side groups, the PPE-Ar-(4+) chains cannot approach closely enough to allow strong  $\pi$ - $\pi$  interchain interactions. In effect, in the PPE-Ar-(4+) aggregates, the  $\pi$ -conjugated chains are only weakly coupled, and consequently, interchain exciton migration is inefficient. Thus, it is likely that, in the cationic polymers, a quencher ion is able to only effectively quench excitons on the polymer chain that it is ion-paired to. The absence of superlinear SV behavior for the cationic PPE-Ar-(4+) polymers also arises due to the weak interchain interactions in the aggregates.

A final point that is subtle, yet significant, involves the details of the quenching behavior of the PPE-Ar- $\text{SO}_3^-$  series. In particular, for PPE- $\text{SO}_3^-$  and PPE-Py- $\text{SO}_3^-$ , fluorescence



**Figure 8.** Color photograph of methanol solutions of PPE-Ar-SO<sub>3</sub><sup>−</sup> CPEs under illumination with near-UV light. From left to right: PPE-SO<sub>3</sub><sup>−</sup>, PPE-Py-SO<sub>3</sub><sup>−</sup>, PPE-Th-SO<sub>3</sub><sup>−</sup>, PPE-EDOT-SO<sub>3</sub><sup>−</sup>, and PPE-BTD-SO<sub>3</sub><sup>−</sup>.

quenching by NDI<sup>2+</sup> is more efficient in H<sub>2</sub>O (where the polymers are aggregated) than in MeOH. This trend reverses in PPE-Th-SO<sub>3</sub><sup>−</sup> and PPE-EDOT-SO<sub>3</sub><sup>−</sup>, where the quenching is much more efficient in MeOH (see Figure 7b, and note [Q]<sub>90</sub> values in Table 2). As discussed above, quenching is most efficient when the CPE chains are strongly aggregated so that interchain exciton migration is efficient. This explains the highly efficient quenching of PPE-SO<sub>3</sub><sup>−</sup> and PPE-Py-SO<sub>3</sub><sup>−</sup> in H<sub>2</sub>O, where  $K_{sv} \approx 10^7 \text{ M}^{-1}$  and  $[Q]_{90} < 1 \mu\text{M}$ . Note that both of these polymers remain relatively strongly fluorescent even in the aggregated state, which indicates that the lifetime of the singlet exciton is not suppressed by aggregation (in fact the exciton lifetime increases in the PPE-SO<sub>3</sub><sup>−</sup> and PPE-Py-SO<sub>3</sub><sup>−</sup>, Table 2).

An important point is that the fluorescence of PPE-Th-SO<sub>3</sub><sup>−</sup> and PPE-EDOT-SO<sub>3</sub><sup>−</sup> is strongly quenched in H<sub>2</sub>O by aggregation. As noted earlier, the aggregation-induced quenching is believed to arise due to rapid nonradiative decay induced by charge transfer in the aggregate excited state (note that the fluorescence of PPE-Th-SO<sub>3</sub><sup>−</sup> decays more rapidly in H<sub>2</sub>O, Table 2). We believe that this aggregation-induced quenching that occurs for PPE-Th-SO<sub>3</sub><sup>−</sup> and PPE-EDOT-SO<sub>3</sub><sup>−</sup> effectively turns off interchain exciton migration. In effect, the fluorescent excitons are efficiently trapped and quenched by the interchain excimer-like states in the aggregates. This turns off interchain exciton diffusion, which is the basis for the highly efficient fluorescence quenching seen in PPE-SO<sub>3</sub><sup>−</sup> and PPE-Py-SO<sub>3</sub><sup>−</sup>.

## Summary and Conclusions

In the course of the present investigation, we have succeeded in synthesizing and characterizing a series of 10 structurally related CPEs featuring anionic (R-SO<sub>3</sub><sup>−</sup>) and cationic (R-N<sup>+</sup>-R-N<sup>+</sup>-R) side groups. The Pd-mediated coupling synthetic methodology was carried out in water, and in each case polymeric materials were obtained; however, the characterization results indicate that the polymerization reactions are more effective for members of the PPE-Ar-SO<sub>3</sub><sup>−</sup> series. By varying the structure of the poly(arylene ethynylene) backbone, it is possible to vary the HOMO-LUMO gap of the polymers, resulting in a series of materials that display absorption at wavelengths ranging from 400 to 550 nm and fluorescence from 440 to 600 nm. As an example of a range of fluorescence wavelengths attained across this series, Figure 8 illustrates the fluorescence emission from dilute methanol solutions of the five PPE-Ar-SO<sub>3</sub><sup>−</sup> polymers. This image clearly shows that the fluorescence colors range from blue for the PPE-SO<sub>3</sub><sup>−</sup> and PPE-Py-SO<sub>3</sub><sup>−</sup>, to green for the PPE-Th-SO<sub>3</sub><sup>−</sup> and PPE-EDOT-SO<sub>3</sub><sup>−</sup>, to orange-red for PPE-BTD-SO<sub>3</sub><sup>−</sup>.

All of the CPEs are soluble in water and polar organic solvents (e.g., DMF, DMSO, MeOH, etc.). The photophysical data suggests that the chains aggregate in water, but in MeOH (and likely in other polar organic solvents as well), the polymers are well solvated such that the optical properties are characteristic of the “molecularly dissolved” chains. The effect of aggregation on the optical properties of the CPEs is most pronounced for the PPE-Ar-SO<sub>3</sub><sup>−</sup> series. In particular, the absorption undergoes a significant red-shift concomitant with aggregation, combined with a red-shift and quenching of the fluorescence. The absorption shift is believed to arise because  $\pi$  stacking between adjacent polymer chains in the aggregates induces the arylene ethynylene units to adopt coplanar conformations, increasing the  $\pi$  conjugation length, whereas the fluorescence changes arise from interchain  $\pi$ - $\pi$  (excimer and exciplex) interactions in the aggregates. The relatively weaker effect of aggregation on the spectroscopic properties of the PPE-Ar-(4+) polymers is believed to arise due to bulky DABCO-based alkylammonium sidegroups, which, due to steric effects, prevent close approach of the polymer chains in the aggregates.

All of the CPEs studied exhibit amplified quenching when exposed to dilute solutions of oppositely charged fluorescence quencher ions; however, the sensitivity of the quenching response varies strongly across the series. The most efficient quenching is seen for polymers that display relatively efficient fluorescence in the aggregated state. This effect is believed to arise because interchain exciton migration with the aggregates is most effective in these systems.

In the course of this work, we have succeeded in synthesizing CPEs that display fluorescence emission at wavelengths spanning a significant portion of the visible spectrum. Such a series can be useful in the development of novel sensory or light emissive materials and devices based on water-soluble conjugated polymers,<sup>3,6,18,38,42,44,48,49</sup> as well as for investigations of fundamental processes such as energy or charge transport in nanostructured polymer films.<sup>50</sup> However, a disappointing result of this work is that CPEs that exhibit fluorescence emission at wavelengths longer than 500 nm (Ar = Th, EDOT, and BDT) are strongly quenched when the polymers aggregate. In each case, the fluorescence quantum yields of the aggregated polymers are less than 1%. In parallel work that will be reported in a forthcoming paper, we have also examined the fluorescence properties of ultrathin films that contain the PPE-Ar-SO<sub>3</sub><sup>−</sup> and/or PPE-Ar-(4+) CPEs and are fabricated by the polyelectrolyte layer-by-layer (LbL) deposition method.<sup>51</sup> Fluorescence studies of LbL films that contain PPE-Ar-SO<sub>3</sub><sup>−</sup> or PPE-Ar-(4+) (for Ar = Th, EDOT, or BDT) reveal that the fluorescence from the polymers in the films is strongly quenched, by analogy to



the findings for the same polymers when they are aggregated in solution.

Additional work is clearly needed to develop CPE systems that are strongly fluorescent in the long-wavelength region of the visible region and retain their high fluorescence efficiency in aggregates and in the solid state. Research efforts toward this goal are the subject of ongoing work in our laboratories.

**Acknowledgment.** We gratefully acknowledge financial support by the U.S. Department of Energy, Basic Energy Sciences (grant no. DE-FG02-03ER15484).

## References and Notes

- Pinto, M. R.; Schanze, K. S. *Synthesis (Stuttgart)* **2002**, 1293–1309.
- Schanze, K. S.; Zhao, X. In *Handbook of Conducting Polymers*; Skotheim, T. A.; Reynolds, J. R., Eds.; CRC Press: Boca Raton, FL, 2006; Vol. 3, in press.
- Kim, S.; Jackiw, J.; Robinson, E.; Schanze, K. S.; Reynolds, J. R.; Baur, J.; Rubner, M. F.; Boils, D. *Macromolecules* **1998**, *31*, 964–974.
- Chen, L.; McBranch, D. W.; Wang, H.-L.; Helgeson, R.; Wudl, F.; Whitten, D. G. *Proc. Natl. Acad. Sci. U.S.A.* **1999**, *96*, 12287–12292.
- Tan, C. Y.; Pinto, M. R.; Schanze, K. S. *Chem. Commun.* **2002**, 446–447.
- Ramey, M. B.; Hiller, J. A.; Rubner, M. F.; Tan, C. Y.; Schanze, K. S.; Reynolds, J. R. *Macromolecules* **2005**, *38*, 234–243.
- Cutler, C. A.; Bouguettaya, M.; Kang, T. S.; Reynolds, J. R. *Macromolecules* **2005**, *38*, 3068–3074.
- Stork, M.; Gaylord, B. S.; Heeger, A. J.; Bazan, G. C. *Adv. Mater.* **2002**, *14*, 361–366.
- Fan, Q. L.; Zhou, Y.; Lu, X. M.; Hou, X. Y.; Huang, W. *Macromolecules* **2005**, *38*, 2927–2936.
- Schnablegger, H.; Antonietti, M.; Göltner, C.; Hartmann, J.; Cölfen, H.; Samori, P.; Rabe, J. P.; Häger, H.; Heitz, W. *J. Colloid Interface Sci.* **1999**, *212*, 24–32.
- Thünemann, A. F.; Ruppelt, D. *Langmuir* **2000**, *16*, 3221–3226.
- Pinto, M. R.; Kristal, B. M.; Schanze, K. S. *Langmuir* **2003**, *19*, 6523–6533.
- Harrison, B. S.; Ramey, M. B.; Reynolds, J. R.; Schanze, K. S. *J. Am. Chem. Soc.* **2000**, *122*, 8561–8562.
- Wang, D. L.; Wang, J.; Moses, D.; Bazan, G. C.; Heeger, A. J. *Langmuir* **2001**, *17*, 1262–1266.
- Tan, C.; Atas, E.; Müller, J. G.; Pinto, M. R.; Kleiman, V. D.; Schanze, K. S. *J. Am. Chem. Soc.* **2004**, *126*, 13685–13694.
- Zhou, Q.; Swager, T. M. *J. Am. Chem. Soc.* **1995**, *117*, 12593–12602.
- Müller, J. G.; Atas, E.; Tan, C.; Schanze, K. S.; Kleiman, V. D. *J. Am. Chem. Soc.* **2006**, *128*, 4007–4016.
- Mwaura, J. K.; Pinto, M. R.; Witker, D.; Ananthakrishnan, N.; Schanze, K. S.; Reynolds, J. R. *Langmuir* **2005**, *21*, 10119–10126.
- Sonogashira, K. In *Comprehensive Organic Synthesis*; Trost, B. M., Fleming, I., Eds.; Pergamon Press: Oxford, 1991; Vol. 3, p 521.
- Bunz, U. H. F. *Chem. Rev.* **2000**, *100*, 1605–1644.
- Muathen, H. A. *J. Chem. Res. Synop.* **1994**, 405–405.
- Takahashi, S.; Kuroyama, Y.; Sonogashira, K.; Hagihara, N. *Synthesis (Stuttgart)* **1980**, 627–630.
- Khan, M. S.; Al-Suti, M. K.; Al-Mandhary, M. R. A.; Ahrens, B.; Bjernemose, J. K.; Mahon, M. F.; Male, L.; Raithby, P. R.; Friend, R. H.; Kohler, A.; Wilson, J. S. *J. Chem. Soc., Dalton Trans.* **2003**, 65–73.
- Bunten, K. A.; Kakkar, A. K. *Macromolecules* **1996**, *29*, 2885–2893.
- Neenan, T. X.; Whitesides, G. M. *J. Org. Chem.* **1988**, *53*, 2489–2496.
- The plots of  $\eta_{sp}/c$  vs  $c$  were nonlinear in the absence of added electrolyte. This effect is believed to result from the polymers acting as “rigid rods” because of strong electrostatic repulsion between the ionic side groups. Addition of 0.1 M LiBr to increase the ionic strength of the solution suppresses intrachain electrostatic repulsion. Under this condition, the polymers are less rigid rod in nature and the viscosity varies such as that of a solution of a random coil polymer, i.e.,  $\eta_{sp}/c$  increases with  $c$ .
- Weder, C., Ed. *Poly(arylene ethynylene)s; From Synthesis to Application*; Springer: Berlin, 2005; Vol. 177.
- Hou, J. H.; Yang, C. H.; Qiao, J.; Li, Y. F. *Synth. Met.* **2005**, *150*, 297–304.
- Li, X. Z.; Zhang, Y.; Yang, R. Q.; Huang, J.; Yang, W.; Cao, Y. *J. Polym. Sci., Part A: Polym. Chem.* **2005**, *43*, 2325–2336.
- Bredas, J. L.; Cornil, J.; Beljonne, D.; dos Santos, D.; Shuai, Z. G. *Acc. Chem. Res.* **1999**, *32*, 267–276.
- Gordon, M.; Ware, W. R., Eds. *The Exciplex*; Academic Press: New York, 1975.
- Young, J. K.; Moore, J. S. In *Modern Acetylene Chemistry*; Diederich, F.; Stang, P. J., Eds.; VCH: Weinheim, 1995; p Chapter 12.
- Kim, J.; Swager, T. M. *Nature* **2001**, *411*, 1030–1034.
- Fiesel, R.; Halkyard, C. E.; Rampey, M. E.; Kloppenburg, L.; Studer-Martinez, S. L.; Scherf, U.; Bunz, U. H. F. *Macromol. Rapid Commun.* **1999**, *20*, 107–111.
- Halkyard, C. E.; Rampey, M. E.; Kloppenburg, L.; Studer-Martinez, S. L.; Bunz, U. H. F. *Macromolecules* **1998**, *31*, 8655–8659.
- Jenekhe, S. A.; Osaheni, J. A. *Science* **1994**, *265*, 765–768.
- Kim, I. B.; Erdogan, B.; Wilson, J. N.; Bunz, U. H. F. *Chem.—Eur. J.* **2004**, *10*, 6247–6254.
- Juan, Z.; Swager, T. M. In *Poly(arylene ethynylene)s: From Synthesis To Application*; Springer: Berlin, 2005; Vol. 177, pp 151–179.
- Wosnick, J. H.; Mello, C. M.; Swager, T. M. *J. Am. Chem. Soc.* **2005**, *127*, 3400–3405.
- Wang, J.; Wang, D. L.; Miller, E. K.; Moses, D.; Bazan, G. C.; Heeger, A. J. *Macromolecules* **2000**, *33*, 5153–5158.
- Gaylord, B. S.; Heeger, A. J.; Bazan, G. C. *Proc. Natl. Acad. Sci. U.S.A.* **2002**, *99*, 10954–10957.
- Liu, B.; Bazan, G. C. *J. Am. Chem. Soc.* **2006**, *128*, 1188–1196.
- Cabarcos, E. L.; Carter, S. A. *Macromolecules* **2005**, *38*, 10537–10541.
- Fan, Q. L.; Zhang, G. W.; Lu, X. M.; Chen, Y.; Huang, Y. Q.; Zhou, Y.; Chan, H. S. O.; Lai, Y. H.; Xu, G. Q.; Huang, W. *Polymer* **2005**, *46*, 11165–11173.
- Greenfield, S. R.; Svec, W. A.; Gosztola, D.; Wasielewski, M. R. *J. Am. Chem. Soc.* **1996**, *118*, 6767–6777.
- Lakowicz, J. R. *Principles of Fluorescence Spectroscopy*; 2nd ed.; Kluwer Academic/Plenum Publishers: New York, 1999.
- Kim, J.; McQuade, D. T.; Rose, A.; Zhu, Z.; Swager, T. M. *J. Am. Chem. Soc.* **2001**, *123*, 11488–11489.
- Baur, J. W.; Kim, S.; Balanda, P. B.; Reynolds, J. R.; Rubner, M. F. *Adv. Mater.* **1998**, *10*, 1452–1455.
- Ma, W. L.; Iyer, P. K.; Gong, X.; Liu, B.; Moses, D.; Bazan, G. C.; Heeger, A. J. *Adv. Mater.* **2005**, *17*, 274–277.
- Baur, J. W.; Rubner, M. F.; Reynolds, J. R.; Kim, S. *Langmuir* **1999**, *15*, 6460–6469.
- Mwaura, J. K.; Müller, J. G.; Kleiman, V. D.; Reynolds, J. R.; Schanze, K. S., to be submitted.
- Kellogg, R. E.; Bennett, R. G. *J. Chem. Phys.* **1964**, *41*, 3042–3045.
- Reynolds, G. A.; Drexhage, K. H. *Opt. Commun.* **1975**, *13*, 222–225.
- Magde, D.; Wong, R.; Seybold, P. G. *Photochem. Photobiol.* **2002**, *75*, 327–334.
- Magde, D.; Brannon, J. H.; Cremers, T. L.; Olmsted, J., III. *J. Phys. Chem.* **1979**, *83*, 696–699.
- Jones, G. II; Jackson, W. R.; Choi, C. *J. Phys. Chem.* **1985**, *89*, 294–300.

MA0611523